The Journal of the Korean Society of
Coastal and Ocean Engineers
Vol. 4, No. 4, pp. 231~242, December 1992

Modeling of Tidal and Wind-Driven Currents in Eastern Coastal Waters of the Yellow Sea
黃海東側 沿岸域의 潮流 및 風成流 模型

Young Jae Ro* and Ik Hwan You*
노영재* · 유익환*

Abstract □ This study uses a numerical model to investigate the circulation patterns of the tidal and wind driven current components. The model is vertically averaged 2-D transient, using explicit numerical scheme, based on equation of motion and continuity, forced by water elevation at open boundaries and wind stress. The model domain extends from 35°N to 36°40′N lat., and 125°E to 126°40′E long. with x, y grid spacing of 5 km. The model reproduces the tide and tidal currents by 4 major constituents successfully with more than 90% accuracy when compared to two offshore tidal records and currents at one offshore measurements for 22 days. Responses of coastal waters to six schematic wind events are analyzed in terms of current distribution patterns and local features. Regardless of wind directions, strong coastal currents were produced. Bottom topography plays a critical role in producing a local eddy field whose center is located offshore Pu An with its major radius of 40 km.

要 旨 : 본 연구에서는 數値模型을 이용하여 潮流 및 吹送流의 순환형태를 고찰하였다. 사용된 모형은 유체의 운동 및 연속방정식에 기초한 연직평균 2차원 모형으로서 陽解法을 사용하며, 개방경계에서의 해수면 변화와 바람의 剪斷力에 의한 forcing을 포함한다. 모형의 영역은 북위 35°~36°40′, 동경 125°~126°40′이며 경사간격은 x, y 방향 공히 5 km이다. 외해측에서 22일간 관측된 조석(2개 지점) 및 조류(1개 지점) 자료와 비교한 결과 본 모형은 4개 주요 分潮에 의한 조석 및 조류를 정확도 90% 이내로 재현하였다. 여섯 가지 경우의 가상적인 바람에 대한 해석을 통하여 흐름의 분포양상과 지역적인 특성을 고찰하였다. 그 결과, 풍향에 관계 없이 강한 沿岸流가 발생하며, 또한 해저지형의 영향으로 부안 외해측에 主半徑 40 km의 지역적인 渦流가 발생함을 확인하였다.

1. INTRODUCTION

Numerical modellings have been applied to a wide area of oceanographic problems including global warming issues, general circulation in the ocean, trajectory of pollutant, oil spill, and search and rescue operation with a reasonable degree of success. These efforts are directed toward two goals, namely academic and practical. More and more, numerical modelling is becoming a powerful and reliable tool in both direction, since the accuracy of model predictions is being verified in many ways and the steps of model calibration have been more rigorously established.

Since the modelling work to reproduce the tide and tidal currents in the Yellow and East China Sea (An, 1977; Choi, 1980), the numerical modelling applications have increased in recent years in many oceanic problems. Those include various water bodies in nearshore, coastal, shelf, slope, sea and basin-scale ocean with subjects concerned with local tide simulation, sediment transport, conceptual and diagnostic modelling of ocean circulation, environmental impact assessment, prediction of heat discharge, etc (Choi, 1984; Choi *et al.*, 1989; Kim *et al.*, 1989; Kim, 1991; Kang *et al.*, 1989; Ro *et al.*, 1991). However, few works have been directed to validate the model with careful calibration of the

*忠南大學校 海洋學科(Department of Oceanography, Chung Nam National University, Taejeon 305-764, Korea)

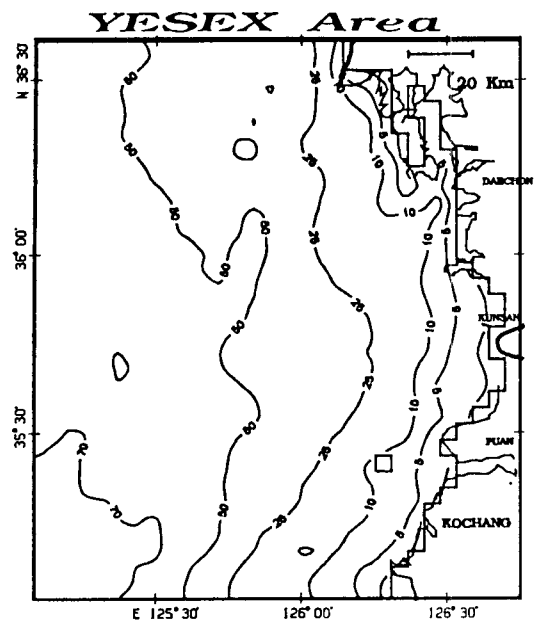

Fig. 1. Modelling domain for the middle section of the West Coast of South Korea with bottom topography.

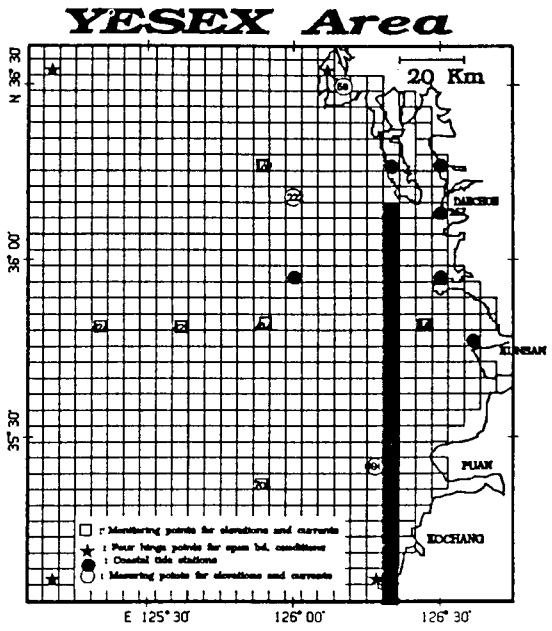

Fig. 2. Model grid system and coastal boundary, 58: Sin Jin-do, 690: Wi-do, 222: Oe Yun-do.

model results by field measurements. This paper presents results from applications of the model to the observed data sets of tide and tidal currents for the purpose of model calibration.

This study investigates coastal currents driven by tide and wind in eastern coastal waters of Korean Peninsula (Fig. 1) by using a 2-D vertically averaged numerical model. Two objectives of the modelling efforts are i) to simulate tide and tidal current, ii) to reproduce wind-driven current and to investigate response characteristics of water body to wind events. The model predictions are calibrated to a high degree of accuracy which can be useful in a certain area of practical applications such as oil spill and rescue operation in the future. This study is extended to Part II in that particle trajectory modelling is carried out and the diffusion/dispersion characteristics are analyzed.

2. MODELLING CONSIDERATIONS

Considerations for the development or selection of model (Sheng *et al.*, 1989) are numerical method, equations solved, time differencing scheme, spatial differencng scheme, horizontal and vertical grid structures, host computer and etc. Based on these considerations in addition to the characteristics of applications, the model we use is 1) vertically averaged 2-D transient, 2) using explicit numerical scheme, 3) based on vertically averaged equation of continuity and motion, 4) forced by water elevation at open boundaries for tide and wind stress at the surface.

Model specifications are as follows; As shown in Fig. 1, the model Domain encompasses 35°-36°40′ N latitude, and 125°10′-126°30′ E longitude with grid spacing of 5 km. Due to the nature of explicit computational scheme used, the time interval of 60 seconds was used to meet the CFL stability criterion. The computational grid system and other important stations for calibration strategy are shown in Fig. 2.

3. NUMERICAL SCHEMES

The vertically averaged governing equations for continuity and current motions are

$$\frac{\delta\eta}{\delta t}+\frac{\delta}{\delta x}(Hu)+\frac{\delta}{\delta y}(Hv)=0 \quad (1)$$

$$\frac{\delta u}{\delta t}+u\frac{\delta u}{\delta x}+v\frac{\delta u}{\delta y}-fv + \frac{ku(u^2+v^2)}{H}+g\frac{\delta\eta}{\delta x}=0 \quad (2)$$

$$\frac{\delta v}{\delta t}+u\frac{\delta v}{\delta x}+v\frac{\delta v}{\delta y}+fv + \frac{kv(u^2+v^2)}{H}+g\frac{\delta\eta}{\delta y}=0 \quad (3)$$

where η is the sea surface elevation and u and v represent vertically averaged velocities such as

$$u=\frac{1}{H}\int_h^\eta u'\,dz \quad v=\frac{1}{H}\int_h^\eta v'\,dz$$

The cartesian coordinates, x and y is increasing eastward and northward positively. H is water column depth $(h+\eta)$, f is coriolis parameter, g is gravitation constant and for friction coefficient, k, the value of 0.0025 was used for all cases.

Finite difference forms of continuity equation, (1) and of linearized equations of motion, (2), (3) are

$$\{\eta_i(t+\tau)-\eta_i(t)\}/\tau=-\{d_i(t)u_i(t)-d_{i-1}(t)u_{i-1}(t) + e_{i-m}(t)v_{i-m}(t)-e_i(t)v_i(t)\}/s \quad (4)$$

$$\{u_i(t+\tau)-u_i(t)\}/\tau=fv(t)-ku_i(t+\tau)\{u_i^2(t)+v_i^2(t)\}/D_i(t) -g\{\eta_{i+1}(t+\tau)-\eta_i(t+\tau)\}/s \quad (5)$$

$$\{v_i(t+\tau)-v_i(t)\}/\tau=fu(t+\tau)-kv_i(t+\tau)\{u_i^2(t)+v_i^2(t)\}/E_i(t) -g\{\eta_i(t+\tau)-\eta_{i+m}(t+\tau)\}/s \quad (6)$$

where $d_i=(H_i+H_{i+1})/2$, $e_i=(H_i+H_{i+m})/2$,
$D_i=\max(d_i, H_o)$, $E_i=\max(e_i, H_o)$
$u_i=1/4(u_{i-1}+u_i+u_{i+m-1}+u_{i+m})$,
$v_i=1/4(v_{i-m}+v_{i-m+1}+v_i+v_{i+1})$

and τ denotes for time increment of 600 seconds. Index notations and other conventions are referred to Flather and Heaps (1975).

4. MODELLING OF TIDE AND TIDAL CURRENT

The predominant coastal current in this area is due to astronomical tide. This study is focusing on the four major tidal constituents, namely M_2, S_2, K_1, O_1. Reproduction of tides and tidal currents in the study area would reguire the specifications of tidal elevations along the three open boundary lines. Of course, the degree of success in reproducing the tide and tidal current depends heavily on the boundary conditions imposed. Thus the task of obtaining the accurate amplitude and phase information is crucial. However, the data source needed for the model calibration is very much limited and mostly confined to the coastal tidal stations. The tidal stations where the tidal records were used for calibration purpose are indicated in Fig. 2. Depths specified at the center of each cell were extracted from bathymetric data gathered from the Navigation chart revised by the Office of Hydrographic Affairs, Korea in 1985. Historical tide data at the open boundary is almost non-existent. Such a situation in modelling works puts a great burden and limitation. Simply, it means that we have to rely on our best guess on the offshore boundary condition. A source we rely on comes from the cotidal and cophase chart by Choi (1980). Yet, these charts are not adequate enough to resolve small local area, since it covers the entire Yellow Sea and East China Sea area. Two island tidal stations, Wi-do (690) and Sin Jin-do (58) provide tidal records in the offshore water area, which are used for the model calibration purpose. The model was started at zero sea surface elevation and tidal forcings were subsequently added at open boundary points with predetermined tidal harmonics. Fig. 3 shows the time series of sea levels at three open boundary points marked in Fig. 2. Table 1 lists the amplitudes and phases for 4 major constituents at the four corner boundary poi-

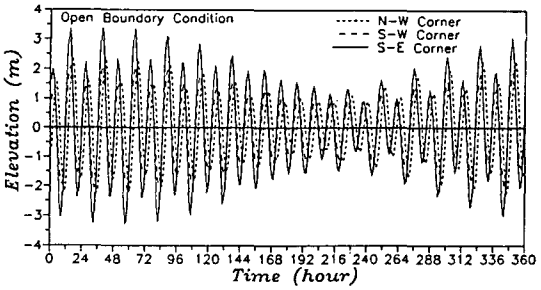

Fig. 3. Time series of tidal elevations imposed at 3 stations on the southern boundary.

Table 1. Amplitude and phase information for the three hinge points on the open boundaries

	Amplitude				Phase			
	NW	NE	SW	SE	NW	NE	SW	SE
M_2	1.46	2.16	1.35	2.00	130.00	118.87	63.75	50.96
S_2	0.54	0.77	0.45	0.85	159.02	151.39	113.65	104.69
K_1	0.30	0.37	0.25	0.40	295.00	292.00	268.00	260.00
O_1	0.18	0.25	0.18	0.33	247.71	245.79	230.44	225.32

Amplitude: (m), Phase: degree relative to 10°N, NW: Northwest, NE: Northeast, SW: Southwest, SE: Southeast point.

nts which were used as boundary forcing. Tidal elevations along the open boundary lines were linearly interpolated between tidal elevations at both end of the lines. Tests of initial model run were conducted with single harmonics of M_2 to find that after 8 cycles, the model produces elevation and current field of a single M_2 harmonic. Therefore we discarded first 8 cycles of model run with multiple harmonics for following works.

In general, compared to tidal records, historical tidal current measurements are much more difficult to be available. As a part of YESEX (Yellow Sea Experiment) I, and for this modelling, we moored current meters at two locations. One is lost and the other could provide 22-day record near Oe Yundo (222), and was used for the calibration of tidal current.

The model outputs were calibrated against parameters and conditions such as surface and bottom friction coefficients, imposed amplitudes and phases of tidal constituents, water elevations and currents at tidal stations and measuring points, and numerical schemes of open boundary radiation condition.

5. MODELLING OF COASTAL CURRENT RESPONSE TO WIND EVENTS

To experiment the coastal current responses to wind events, two schemes are setup. First, we investigate the response with three different bottom topographies (i.e., flat, linearly sloping and realistic). Second, responses to steady wind of 10 m/sec and/or time varying wind with three wind directions are analyzed, respectively. The varying wind is linearly increasing from start to 1.5 days upto 10 m/sec and then decreasing to no wind for next 1.5 days. The wind field in the study domain is assumed to be homogeneous which reflect the mesoscale atmospheric field. Sensitivity analyses are also conducted with respect to drag coefficients of 0.625×10^{-3}, 1.25×10^{-3}, 2.50×10^{-3}.

For the specifications of open boundary conditions on three sides, the Orlansky-type radiation condition was implemented in explicit form so that the disturbances inside the computational domain is freely passing across the boundaries. Numerous numerical schemes of radiation conditions have been reported and their roles have been investigated by Chapman (1985) and Roed and Cooper (1986, 1987). After testing conditions such as clamped, gradient, Orlansky-type radiation condition, we decided to use the Orlansky-type which is adequate for our experimental purposes.

6. RESULTS OF THE NUMERICAL EXPERIMENTS

6.1 Tide

The results of tide are presented in terms of amplitude and phase characteristics. Fig. 4 shows the coamplitude and cophase chart of 4 major tidal constituents, respectively. The chart of the most dominant M_2 constituent, Fig. 4a shows that the amplitudes increase from offshore to inshore direction and in general are parallel with the coast line. The M_2 amplitudes in this area ranges from 1.4 to 2.1 meters. The An Myeon-do and Dae Chon area with more than 2.1 m is known to have the highest tidal range in this area. The cophase map of M_2 drawn in dotted line in Fig. 4a shows that the phases are increasing from south to northward direction. The contour level, 7.2 degree for M_2 tide corresponds

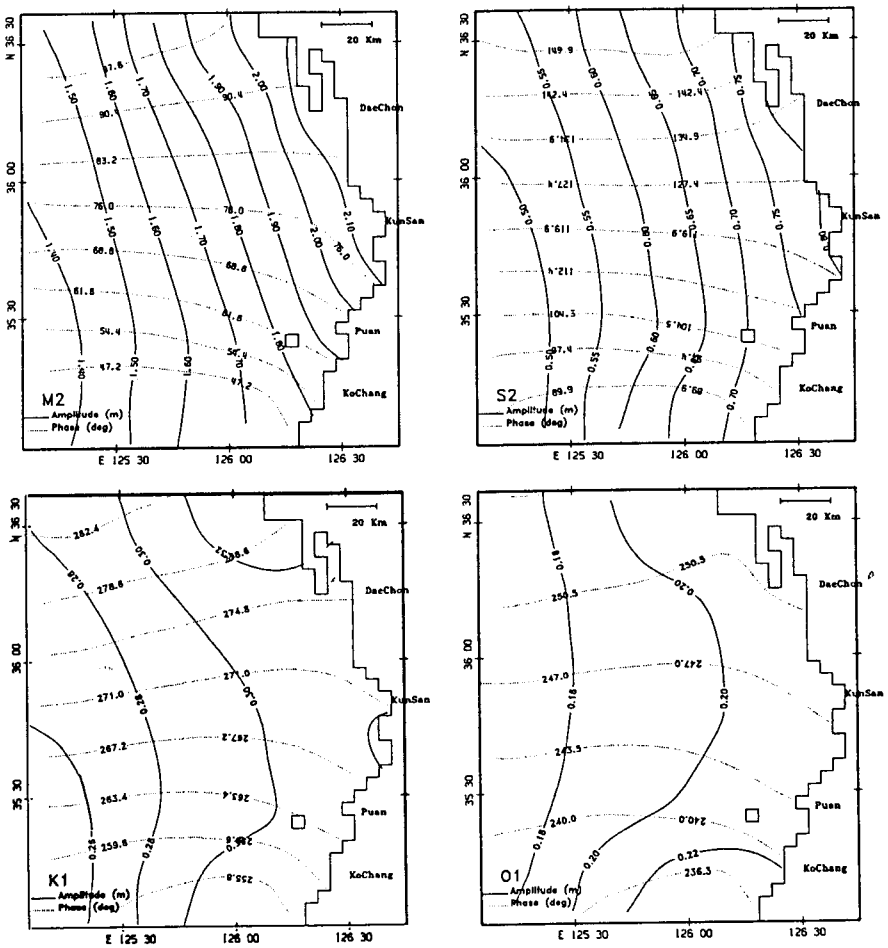

Fig. 4. Computed tidal chart in the study area. A: M_2, B: S_2, C: K_1, D: O_1.

to 15 minute so that it would take approximately two hours for tidal wave to propagate from the southern boundary to the northern one. The cophase and coamplitude charts show the similar characteristics between semidiurnal constituents and diurnal constituents respectively.

Fig. 5 shows the time series of sea level at Wi-do and Sin Jin-do which are calibrated to the in situ measurements (shown in dotted line), which feature general semidiurnal variation as well as neap-spring modulation. The calibration results are summarized in Table 1. The modelled results agree quite well with the observed records in terms of amplitudes, phase, and phase lags between Sin Jin-do and Wi-do. For amplitudes, the model reproduces with more than 95% accuracy except for O_1 at Wi-do. For phases, the model is accurate with less than 2.6° which is corresponding to 2.1% relative error. The greatest difference between observed and modelled amplitude among 4 major constituents is 7 cm at Wi-do. The phase lag information should be considered to be a most important criterion in evaluating the model response, since it reflect the propagation characteristics of the tidal wave. The model is very successful in M_2 phase lag, while the overall results are quite acceptable with less than 2-degree differences.

6.2 Tidal Currents

Fig. 6 shows the horizontal distribution of tidal currents at flood and ebb conditions at their strongest phases. The flooding currents are toward nor-

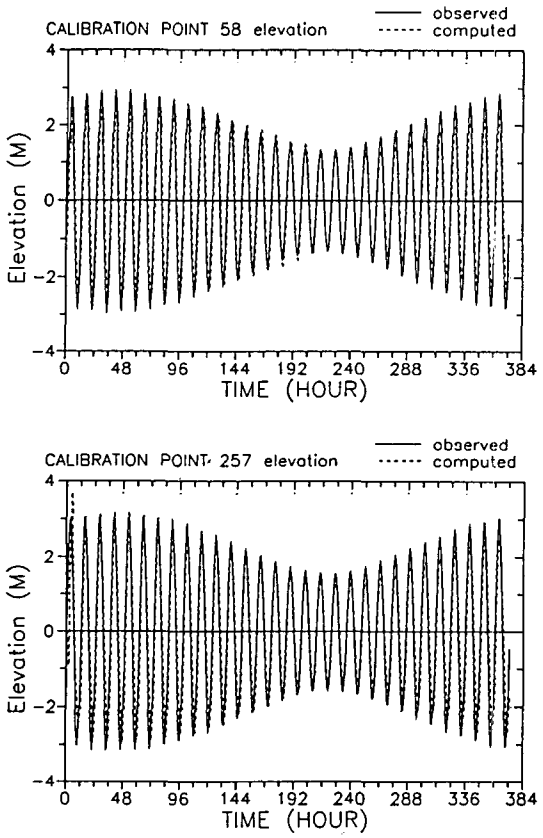

Fig. 5. Time series of the tidal elevation reproduced from the model.

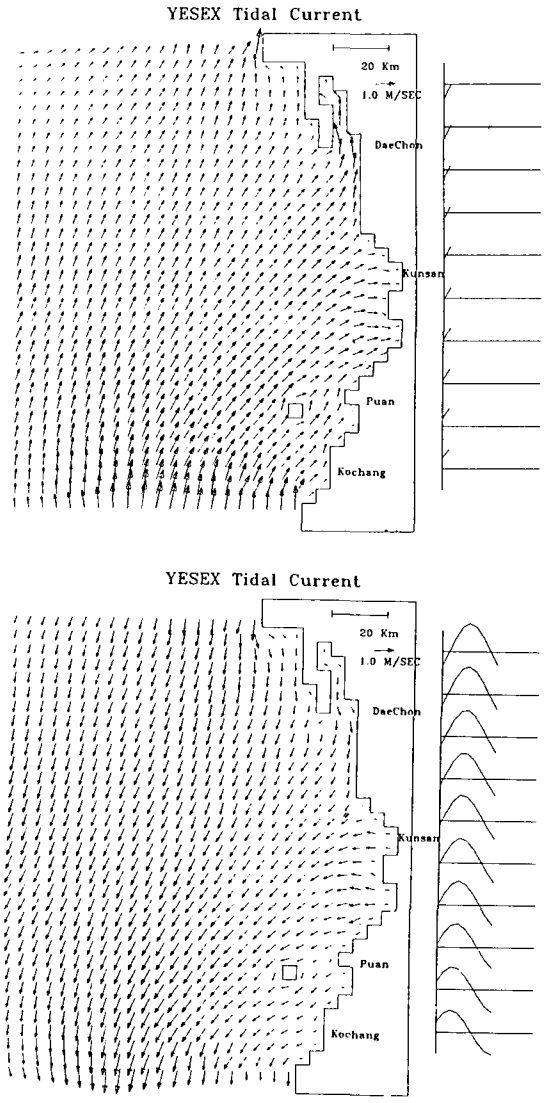

Fig. 6. Horizontal distribution of tidal current reproduced from the model, A: at flood condition, B: at ebb condition.

theast near the coastline and almost northward at offshore. The ebbing currents are almost opposite in direction with similar magnitude of speeds. These features are summarized in Fig. 7 which shows the tidal current ellipses of 4 constituents. M_2 tidal ellipses are characterized so that at the center of domain, ellipses are more circular than those near coastal and offshore boundaries and the principal axis at offshore is north-south, while that at inshore is northeast-southwest. Compared to M_2 ellipses, other ellipses are much smaller in their axis lengths (current speed).

To show the time variation of tidal current and its comparison to measured current, Fig. 8 is prepared for 222 point (near Oe Yun-do). The absolute magnitude of reproduced tidal current is 68.8 cm/sec compared to that of measured one, 68.3 cm/sec which are in an excellent good agreement. However, the comparison in terms of u, v components are relatively poor. The reproduced u and v components are 30.2 and 62.5 compared to the observed ones of 21.7 and 65.2 cm/sec. This is understood that the reproductions of the east-west u component are more exaggerated due to big tidal ranges existing in relatively small region so that currents are deflected toward coastline. To overcome this, more accurate open boundary information are required.

Table 2. Amplitude and phase information at Sin Jin-do and Wi-do from tidal records and modelling results

		Observed		Modelled		Obs.-Mod.		R.E.		Phase Lag	
		Amp.	Phase	Amp.	Phase	Amp.	Phase	Amp.	Phase		
SINJINDO	M_2	2.16	96.90	2.11	96.40	0.05	0.55	2.30	0.57		
	S_2	0.73	137.70	0.75	137.50	−0.02	0.18	−2.90	0.13		
	K_1	0.32	281.20	0.34	281.50	−0.02	−0.25	−4.70	−0.09		
	O_1	0.22	254.40	0.22	254.80	0.00	−0.36	0.90	−0.14		
WIDO	M_2	2.00	67.90	1.92	67.50	0.07	0.42	3.60	0.62	29.00	28.87
	S_2	0.73	117.90	0.75	120.50	−0.03	−2.57	−3.60	−2.18	19.80	17.05
	K_1	0.34	265.90	0.31	267.00	0.03	−1.12	9.10	−0.42	15.35	14.48
	O_1	0.25	244.60	0.21	246.40	0.04	−1.83	15.40	−0.745	9.82	8.35

Amp: Amplitude (m), Phase: degree, R.E.: Relative Error (%)=(Obs.-Mod.)×100/Obs., Phase Lag=Phase at Sin Jin-do-Phase at Wi-do (deg).

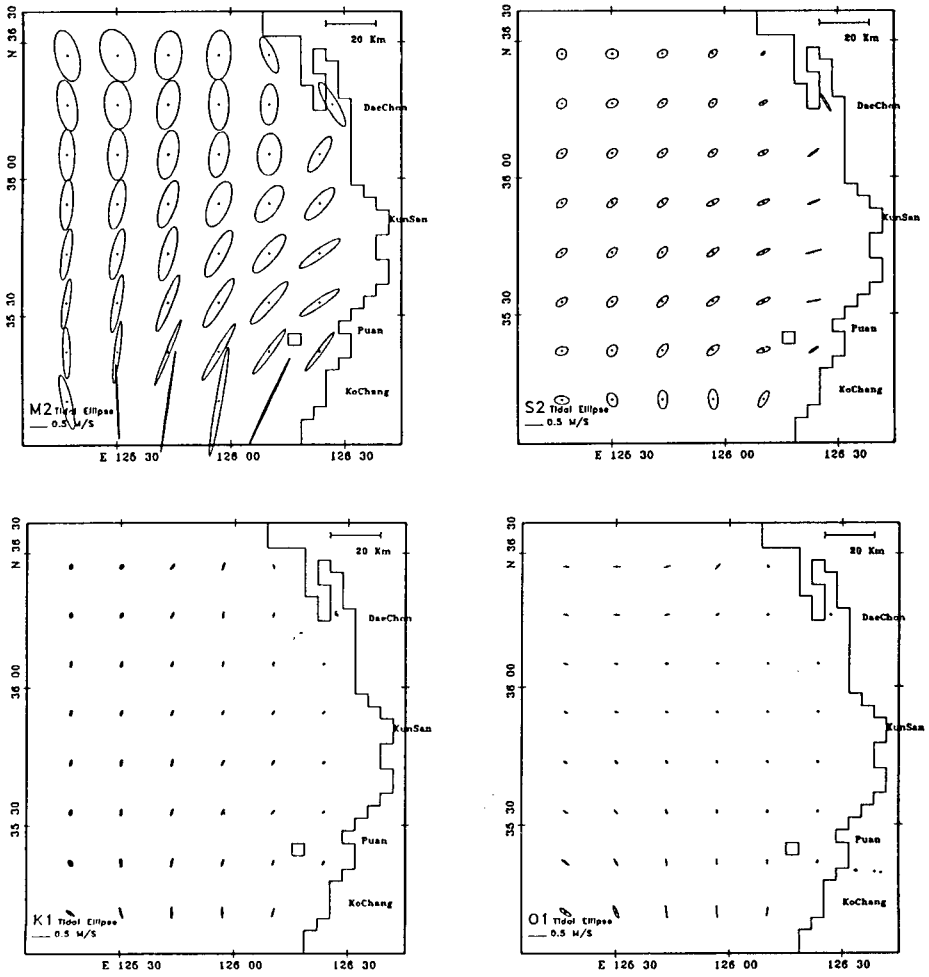

Fig. 7. Tidal ellipses of M_2, S_2, K_1 and O_1 tidal constituents.

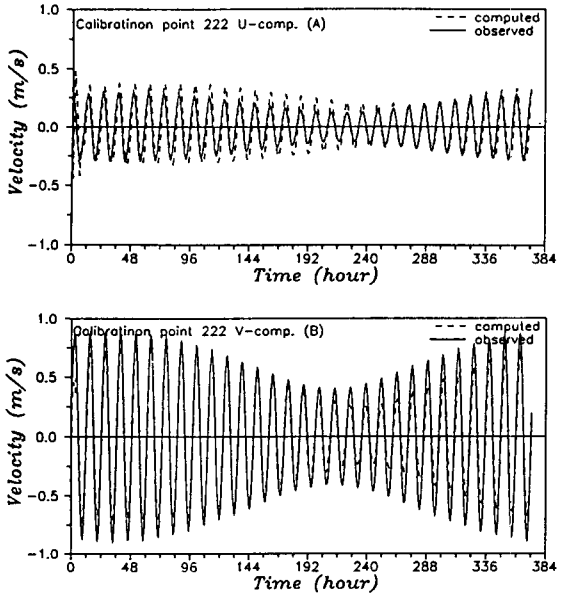

Fig. 8. Comparison of reproduced tidal currents to the measured one at the point of 222 near the Oe Yondo. A for u component and B for v component.

6.3 Wind-driven Currents

The responses of sea surface elevation and currents to wind are pretty sensitive to the drag coefficients (0.625×10^{-3}, 1.25×10^{-3}, 2.50×10^{-3}) in Fig. 9. The choice of values for drag coefficient has been studied and investigated. However, we do not have solid criteria to choose, yet. Thus, as is most frequently used, the value of 1.25×10^{-3} was used for following modelling.

The responses of coastal current under the steady wind stresses to three conditions of bottom topography are seen in Fig. 10. For the flat bottom, we used 50-meter depths for the entire domain, while linearly sloping bottom depths are specified as 5 meters at the reference line near coastal boundary with 2.5 meters decreasing for each grid distances toward the western boundary. For these experiments, steady westerly wind of 10 m/sec is blowing for three days and then stops. For the flat bottom, a simple current field is developed with dominant southeast direction in Fig. 10a. This case simply reflects the classical Ekman current which deviates 45° to the right from the wind direction. For the sloping bottom, the current field are almost south-

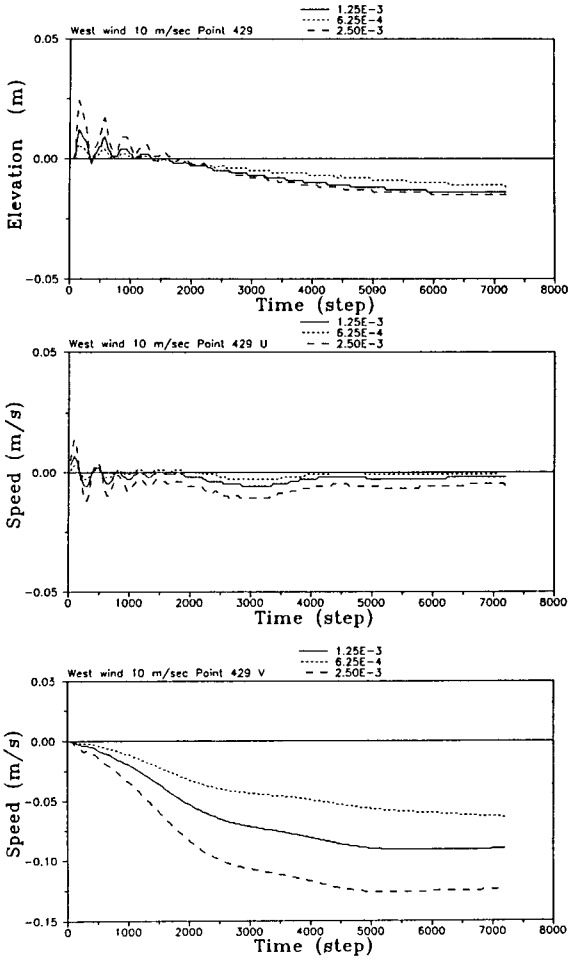

Fig. 9. Responses of sea surface elevation, current velocities to the westerly wind of 10 m/sec with three different drag coefficients (0.625×10^{-3}, 1.25×10^{-3}, 2.50×10^{-3}).

ward with the biggest current in nearshore area in Fig. 10b. Under the steady wind stress, geostrophic current is produced which is parallel with bottom topography. With the realistic bottom depths specified, the current field is changed dramatically (Fig. 11 middle). The field is divided into two regimes, i.e. offshore and inshore ones. In the offshore waters, the response is almost similar to Fig. 10b, while in inshore waters, the field is dominated by the existence of the local eddy field. It is obvious that bottom topography plays a very critical role in producing local eddy, to change the inshore current field. The eddy field will be discussed more in detail

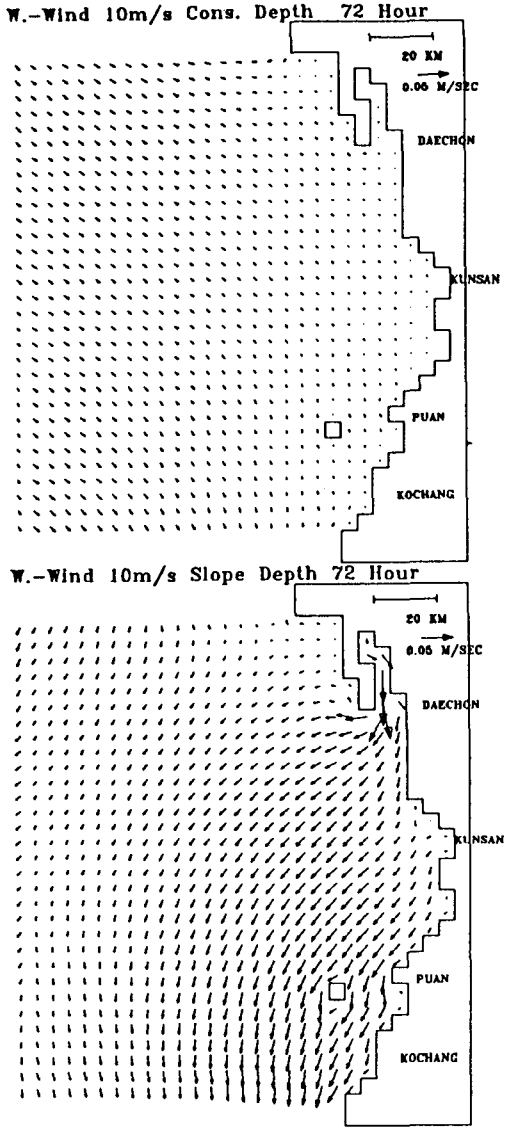

Fig. 10. Responses of coastal currents to the steady westerly wind of 10 m/sec with different bottom topography. A: for flat bottom of 50 meters, B: linearly sloping bottom.

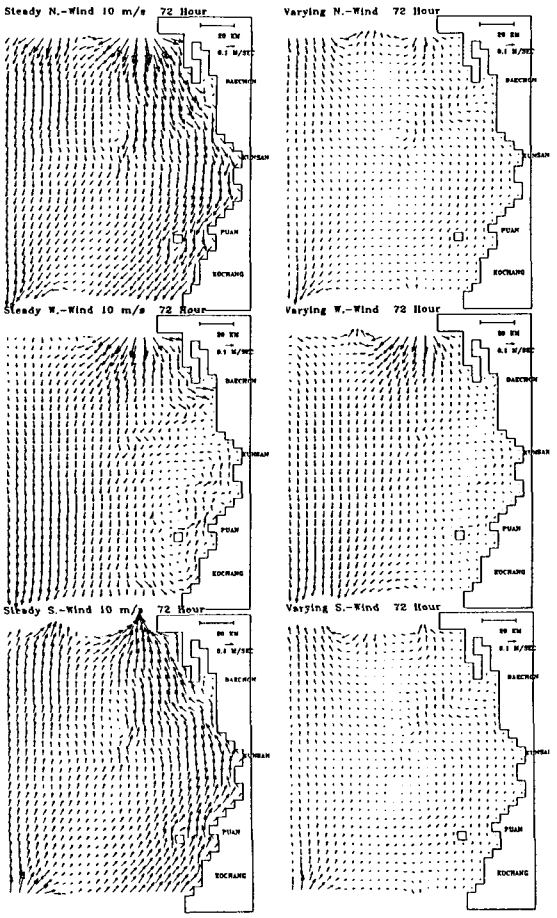

Fig. 11. Wind-driven current fields with steady wind with 10 m/sec (left column) and varying wind (right column). Top: Northerly, middle: Westerly, bottom: Southerly wind.

in later section.

To investigate the response characteristics of coastal current to different wind events, six experiments were setup. We imposed constant wind stresses (pulse type) for three days for northerly, westerly and southerly winds. The other three experiments were under slowly time-varying stresses (STV type). The results of these six experiments are presented to show the responses after three days of wind's blowing in Fig. 11. Left column of figures represents pulse type cases, while right column represents STV type cases. Northerly and southerly winds develop the current fields which are exactly opposite in current directions with same magnitudes of speeds. Currents at inshore waters near the coastline are pretty strong with more than 30 cm/sec. Regardless of wind directions, strong and prominent coastal currents are generated which are the results of water pile-up at the coastal boundary. Under the steady wind stresses, the current fields are adjusted in such a way that the pressure gradient (in this case sea level slope due to water pile-up) is balanced by the

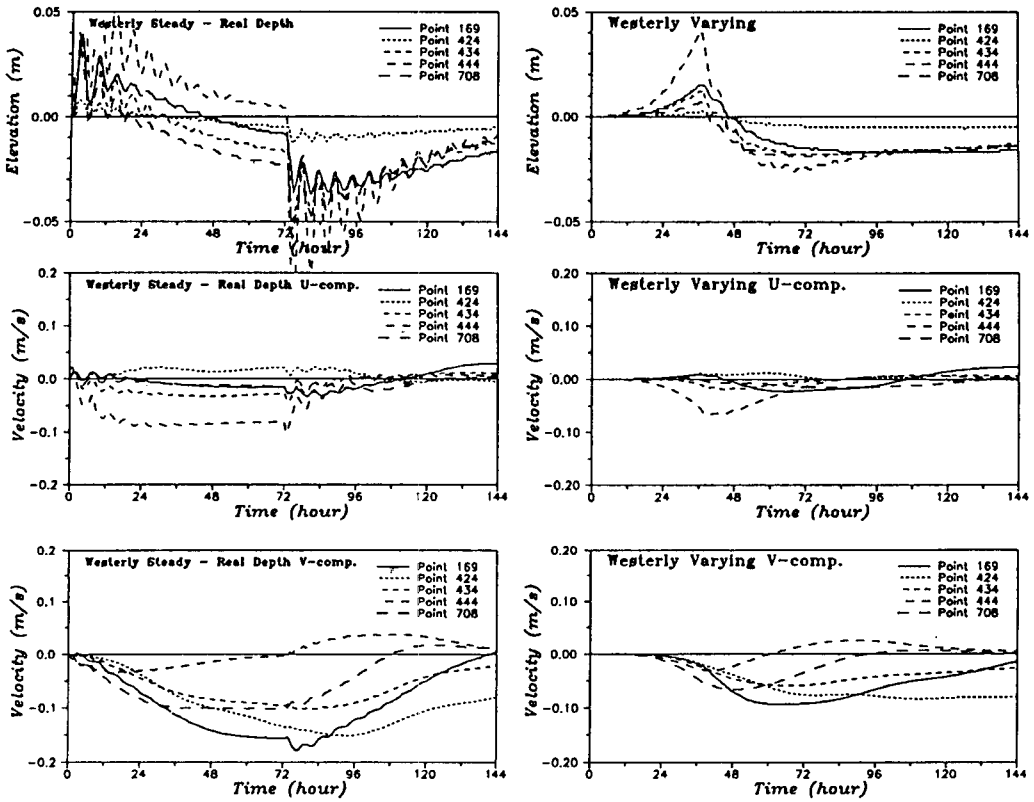

Fig. 12. Time series of modelled sea level, and velocities driven by A: steady wind of 10 m/sec, B: varying westerly wind.

Coriolis force to generated steady geostrophic coastal currents (Chapman, 1985). This is similar to the case of Fig. 10b.

For the case of westerly wind (middle of Fig. 11), a feature of coastal eddy is prominent with its center located offshore Pu An. This feature has not yet been verified with in situ current measurements. However, we have some supporting arguments for the dynamical mechanism. First, it is worthy to note the location of the eddy's center near Pu An where the coastline is curved toward the Kun San area. This geographic condition produces cyclonic eddying motions. This feature exists also in the tidally induced residual currents to be presented in the Part II in a separate paper (Ro and You. 1992). This can be interpreted that the onshore flow component travelling across the isobath experiences water column shrinking (depth decreases) so that it should generate positive relative vorticity in conserving the absolute vorticity. It should be necessary in the future to observe such a local eddy field with field measurements, since it would have very significant implicants for pollutant transports introduced from the Keum River Estuary near the Kunsan area.

Compared to the steady wind stresses, the distribution patterns of the wind-driven currents for STV type are very similar to weaker current speeds.

The characteristics of time variation of the responses of currents to the wind events are presented in Figs. 12. Only westerly cases are presented, since their behaviors are rather similar to the other events of different wind directions. The responses of sea surface elevations to the pulse and PTV type wind stresses are seen in the top panel of Fig. 12. By imposing sudden wind stress or removing it, the sea surface is quickly bulged/lowered and then begins to oscillate until it reaches equilibrium state.

This is due to the sudden increase/decrease of potential energy of water column. To the STV, the response of sea surface is much more moderate so that the water surface increases coherently with the phase of wind stress imposed. The responses of current velocities are similar to water elevation, yet with phase lags. The magnitude of north-south component reaches more than 30 cm/sec, much bigger than east-west component.

7. Conclusions

This modelling study simulates the tide and tidal current in the western coastal waters of middle secton of the Korean Peninsula. Tidal simulations are successful with more than 90% accuracy in terms of amplitudes and phases for 4 major constituents in comparison with two offshore tidal records. Tidal current simulation is also successful, when compared with offshore current measurements in terms of the magnitudes of speed, but not so with u, v components. Reproduced tidal currents show deflected toward costal boundary where local high tidal ranges exist.

Responses of coastal currents to six wind events were investigated. Those results can be summarized; 1) Depending on the types of wind events, southward steady currents are produced in northerly and westerly wind, while in southerly wind event, northward current is produced. They are basically geostrophic in nature showing flows parallel to isobath. 2) Regardless of wind direction, strong currents are produced in inshore waters, 3) Bottom topography plays a critical role in producing local eddy field in westerly wind event. The eddy field produced can be explained under the absolute vorticity conservation argument and as local geography induced eddying motion. This should be investigated in the future with field observations.

This study can be extended to investigate the interaction between tidal and wind-driven currents. Tidally induced residual currents will be investigated to analyze their roles in net transport of pollutants introduced.

REFERENCES

An, H.S., 1977. A numerical experiment of the M_2 tide in the Yellow Sea, *J. Ocean. Soc. Japan*, **33**: 103-110.

Chapman, D.C., 1985. Numerical treatments of cross-shelf open boundaries in a barotropic coastal ocean model, *J. Phs. Oceanogr.* **15**(8): 1060-1075.

Choi, B.H., 1980. A tidal model of the Yellow Sea and the Eastern China Sea, Korea Ocean Res. Develop. Inst. BSPI 00019(3)-36-2 72 p.

Choi, B.H., 1984. Computation of currents driven by a steady uniform wind stress on the East China Sea using a three-dimensional numerical model, *J. Oceanol. Soc. Korea*, **19**(1): 36-43.

Choi, B.H., Kang, K.G. and Lee, S.W., 1989. Tide and sediment transport in the Keum River Estuary, *J. of the Korea Soc. Coastal and Ocean Eng.* **1**(1): 31-43.

Davies, A.M., 1976. A numerical model of North Sea and its use in choosing locations for the deployment of offshore tide gauges in the JONSDAP 76 oceanographic experiment, Deutsche Hydro. *Zeits*, **29**: 11-24.

Flather, R.A. and Heaps, N.S., 1975. Tidal computations for Mocambe Bay, *Geophys. J. Roy. Astro. Soc. 42*: 489-517.

Greenberg, D.A., 1979. A numerical model investigation of tidal phenomena in the Bay of Fundy and Gulf of Maine, *Marine Geodesy*, **2**(2): 161-187.

Kang, S.K., Lee, S.R. and Yum, K.D., 1991. Tidal computations of the East China Sea, the Yellow Sea and the East Sea, Oceanography of Asian Marginal Seas, Elsevier Oceanography Series 54, ed. by K. Takano, pp. 25-48.

Kantha, L.H., Blumberg, A. and Mellor, G., 1985. Computing phase speeds at open boundary, *ASCE J. Hydrau. Eng.*, **116**(4): 592-597.

Kim, C.S., Lee, J.C., Jung, T.S. and Kang, S.H., 1989. Application of 3-d hydrodynamic model, *Ocean Res.* **11**(1): 45-55.

Kim, Y.E., 1991. A numerical study on the circulation of the East Sea (Japan Sea). Ph. D. Disseration Thesis, Seoul National Univ. 211 p.

Ro, Y.J., Kim, T.I., Seung, H.K. and Lee, S.W., 1991. 3-D modelling of heat discharge from Ul-Jin Power Plant into coastal waters of Korea East Sea, Proc. of Estuarine and Coastal Modelling 2nd Intl. Conference/WW Div., ASCE, Tampa, Florida/Nov. 13-15, 1991, pp. 501-512.

Ro, Y.J. and You, I.H., 1992. Numerical investigation of coastal currents and pollutant transport in eastern coastal waters of the Yellow Sea, Modelling of pollutant transport and diffusion with tidal and wind-driven currents. to be submitted to *J. Korean Soc. Coastal and Ocean. Eng.*

Roed, L.P. and Cooper, C.K., 1986. Open boundary conditions in numerical ocean models, *In*: Advanced Physical Oceanographic Modelling, Ed. J.J. O'Brien, NATO ASI Series C: Mathematical and Physical Sciences Vol. 186, D. Reidel Publ. Co., Holland, 411-436.

Roed, L.P. and Cooper, C.K., 1986. A study of various open boundary conditions for wind-forced barotropic

numerical ocean model, *Coastal Eng.,* **11**: 603-637.

Sheng, Y.P., Lee, H.-K. and Wang, K.H., 1989. On numerical strategies of estuarine and coastal modeling, Proc. of Estuarine and Coastal Modeling 1st Intl. Conference/WW Div., ASCE, New Port/Rhode Island/Nov. 15-17, 1989, 291-391.

Wang, J., Blumberg, A. and Butler, H., 1990. Transport prediction in partially stratified tidal water, *Technical Rep., ASCE HY* **116**(3): 380-396.